Proceedings of the 21st ICSMGE, Vienna, Austria, 14 – 19 June 2026. Pistrol, Adam & Schweiger (eds.)
Published by: ÖGG, Austrian Society for Geomechanics, Salzburg, Austria, ISBN 978-3-9503898-4-5
https://doi.org/10.53243/ICSMGE2026-2305

Random finite element analysis on self-supported retaining wall of cement-treated soil columns

Tsutomu Namikawa
Shibaura Institute of Technology, Tokyo, Japan, namikawa@shibaura-it.ac.jp

ABSTRACT: This study presents the random finite element method (RFEM) analysis on the self-supported retaining wall consisting of the cement mixing columns. The wall type improvement used as the retaining wall was simulated and its bending failure behavior was investigated in this analysis. The depth of the excavation at the failure was calculated for the depth-width 1 m wall. The cement mixing columns were modelled as solid elements. The active Rankin earth pressure was applied at the back of the wall and spring elements were used as a subgrade reaction of the excavation side ground. In the RFEM analysis, realizations of the spatial distributions of the unconfined compressive strength q_{uf} of cement-treated soils were generated by the random field theory and the FEM analysis was performed for the generated realizations. The RFEM analysis results showed that the probability distribution of the depth of the excavation at the failure varies with the autocorrelation distance of q_{uf}. The probability distribution of the depth of the excavation at the failure can be used in the reliability-based design of the cement-treated soil wall

KEYWORDS: Deep mixing method, Retaining wall, Spatial variability, RFEM, Reliability-based design.

1 INTRODUCTION

Deep cement mixing (DCM) walls has been adopted as the retaining wall in excavating projects. There are two type of DCM walls for excavation: reinforced and unreinforced. If a slender DCM wall can be adopted as the unreinforced retaining wall, the space constraint and construction cost can be reduced. When an unreinforced DCM wall is used as the retaining wall, the failure behavior of the cement-treated soil wall must be considered in the design procedure. Especially, the bending failure of the wall is a critical issue for the unreinforced DCM wall because the tensile strength of the cement-treated soils is much less than its compressive strength.

Several studies investigated the behavior of the unreinforced DCM walls for excavation (e.g., Jamsawang et al. 2017, Waichita et al. 2019). Jamsawang et al. (2017) conducted a 3D finite element analysis to investigate the behavior of the unreinforced DCM wall in the excavation of soft Bangkok clay. These previous studies investigated the horizontal displacement of the DCM wall, but there are no studies on the failure behavior of the unreinforced DCM wall.

The strength of the ground improvement by DCM varies spatially due to in-situ soil variations and cement slurry mixing variations. Several past studies conducted the random finite element method (RFEM) analysis (Fenton and Griffiths 2008) to investigate the spatial variability of the strength on the behavior of the ground improvement by DCM (e.g., Liu et al. 2015; Pan et al. 2018; Toraldo et al. 2018; Namikawa 2021; Namikawa 2022). In the RFEM analysis, the FEM analysis is incorporated with the random field theory and the Monte Carlo simulation is performed for realizations generated with the random field theory. The past RFEM analysis results indicated that the spatial correlation of the strength affects the behavior of the ground improvement by DCM considerably.

This paper presents a RFEM analysis to evaluate the failure behavior of the unbraced-unreinforced DCM wall. The RFEM analysis is conducted for evaluating the failure behavior of the single-row DCM wall. The mean μ_{quf} and coefficient of variation V_{quf} of the unconfined compressive strength q_{uf} of the cement-treated soil are set to be 2 MPa and 0.3. The autocorrelation distance θ_{quf} is set to be 0.2 m and 1.0 m. The excavation depth at which the overall bending failure occurs is calculated for each realization in the RFEM analysis. The RFEM analysis result provides the failure probability at each excavation depth. Thus based on the RFEM analysis results, the failure probability required in a reliability-based assessment can be assessed at each excavation depth.

2 NUMERICAL ANALYSIS CONDITION

2.1 *Ground condition*

The self-supported DCM wall considered in this study is shown in Figure 1(a). The analysis was performed for the single-row DCM wall of 1 m wide in the homogeneous soil layer. The depth of the DCM wall is 9 m and the ground water table is deeper than 9 m. It was assumed for the soil layer that the density ρ_t = 1.8 g/cm^3, the N-value N = 10, the friction angle ϕ' = 30° and the cohesion c' = 0. The depth of excavation was varied in 0.1 m increments in the numerical analysis. The loading and boundary conditions are shown in Figure 1(b). The active earth pressure σ_A based on Rankine's earth pressure theory was applied at the excavation backside and the horizontal subgrade reaction was used as the resistance at the excavation side. The earth pressure calculated by subtracting the earth pressure at rest σ_R from σ_A was applied at the backside below the excavation level.

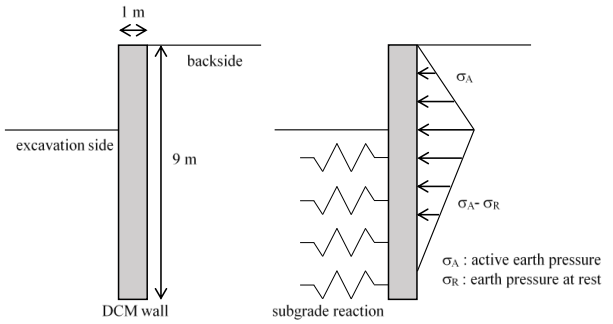

Figure 1. Self-supported DCM wall to be considered in this study. (a) dimension of DCM wall (b) loading condition.

2.2 *Random field of strength of DCM column*

The probability distribution of q_{uf} of the DCM column follows the multivariate lognormal distribution as follow:

$$p\left(\mathbf{q_{uf}}\middle|\mu_{\ln quf}, \sigma^2_{\ln quf}, \theta_{\ln quf}\right) = \frac{1}{\sqrt{(2\pi)^m \left(\sigma^2_{\ln quf}\right)^m |\mathbf{C}| \prod_{i=1}^{m} q_{uf}(\mathbf{r_i})}} \quad (1)$$

$$\exp\left\{-\frac{1}{2\sigma_{\mathrm{lnquf}}^2}\left(\mathbf{lnq_{uf}}-\boldsymbol{\mu}_{\mathbf{lnquf}}\right)^T\mathbf{C}^{-1}\left(\mathbf{lnq_{uf}}-\boldsymbol{\mu}_{\mathbf{lnquf}}\right)\right\}$$

$$\mathbf{q_{uf}}=\begin{bmatrix}q_{\mathrm{uf}}(\mathbf{r_1})\\ \vdots \\ q_{\mathrm{uf}}(\mathbf{r_m})\end{bmatrix},\ \mathbf{lnq_{uf}}=\begin{bmatrix}\ln q_{\mathrm{uf}}(\mathbf{r_1})\\ \vdots \\ \ln q_{\mathrm{uf}}(\mathbf{r_m})\end{bmatrix}$$

$$\boldsymbol{\mu}_{\mathbf{lnquf}}=\begin{bmatrix}\mu_{\mathrm{lnquf}}\\ \vdots \\ \mu_{\mathrm{lnquf}}\end{bmatrix},$$

$$\mathbf{C}=\rho_{\mathrm{lnquf}}(\mathbf{d})=\exp\left(-\frac{\left|\mathbf{r_i}-\mathbf{r_j}\right|}{\theta_{\mathrm{lnquf}}}\right)$$

where m denotes the number of q_{uf} values, μ_{lnquf} denotes the mean of ln q_{uf}, σ_{lnquf} denotes the standard deviation of ln q_{uf}, θ_{lnquf} denotes the autocorrelation distance of ln q_{uf}, $\mathbf{r_i}$ denotes the spatial vector at point i, and $\mathbf{C}$ denotes the correlation coefficient matrix. The spatial correlation of q_{uf} is represented with an exponential autocorrelation function. It was assumed that the mean of q_{uf}, μ_{quf} = 2 MPa and the standard deviation of q_{uf}, σ_{quf} = 0.6 MPa; the coefficient of variation of q_{uf}, V_{quf} = 0.3. The values of μ_{lnquf} and σ_{lnquf} in Equation (1) are calculated form μ_{quf} and σ_{quf} as follow:

$$\sigma_{\mathrm{lnquf}}=\sqrt{\ln\left\{1+\left(\frac{\sigma_{\mathrm{quf}}}{\mu_{\mathrm{quf}}}\right)^2\right\}}$$
$$\mu_{\mathrm{lnquf}}=\ln\mu_{\mathrm{quf}}-\frac{1}{2}\sigma_{\mathrm{lnquf}}^2 \quad (2)$$

It was assumed that the autocorrelation distance with respect to ln q_{uf} corresponds to the autocorrelation distance θ_{quf} with respect to q_{uf}. θ_{quf} was set to be 0.2 m and 1.0 m. The realizations of the random field of q_{uf} were generated by the covariance matrix decomposition method. The random variables for q_{uf} in the random field are assigned to elements in the FEM analysis.

2.3 *Finite element analysis condition*

Three-dimensional FEM analysis was performed using the FEM software DIANA. A part of the single-row DCM wall as shown in Figure 2 was modeled using the finite element mesh. One side of the eight-node isoparametric elements is 100 mm. The bottom surface is fixed in z-direction and the side perpendicular to the load direction is fixed in x-direction. The active earth pressure at the backside was applied as the nodal forces. The horizontal subgrade reaction at the excavation side was modelled as the elastoplastic spring.

An elastoplastic model proposed by Namikawa and Mihira (2007) was used for the cement-treated soil that constitutes the DCM wall. The material parameters of the elastoplastic model in this analysis is listed in Table 1. These parameters for q_{uf} = 2 MPa were based on the previous studies (Namikawa and Mihira 2007). The elastic modulus E, the cohesion c', the tensile strength T_{f} and the fracture energy G_{f} were regarded as the stochastic parameters. These parameters vary in proportion to q_{uf}. The friction angle ϕ', Poisson's ratio ν, the hardening parameters α and e_{y}, the softening parameter e_{r}, the dilatancy coefficient D_{c}, the localization size t_{s0}, and the characteristic length l_{c} are the deterministic parameters. These parameters are held at the values listed in Table 1.

The horizontal subgrade reaction coefficient k_{h} was determined using the relationship between N and k_{h} proposed by Honjo et al. (2005). They proposed the following relationship:

$$k_{\mathrm{h}}=k_{\mathrm{c}}y^{-0.5}$$
$$k_{\mathrm{c}}=217+191N\pm167\ (\mathrm{kN/m^{2.5}}) \quad (3)$$

Assuming the horizontal displacement of the ground surface y = 1 mm, k_{h} was set to be 67000 kN/m^3 for N = 10. The maximum value of the horizontal spring force was set to be the difference between the passive earth pressure and the earth pressure at rest.

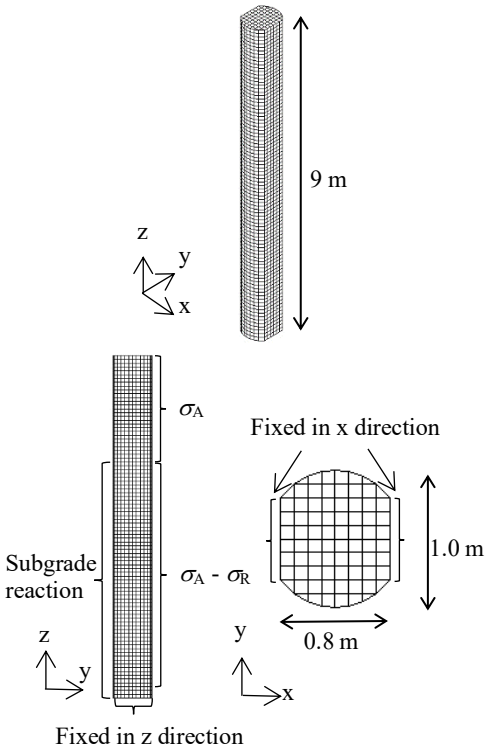

Figure 2. Finite element mesh and boundary conditions in finite element analysis.

Table 1. Material parameters for DCM columns with q_{uf} = 2 MPa.

Parameter	Stochastic or Deterministic	Value
Elastic modulus E	Stochastic	3520 MPa
Poisson's ratio ν	Deterministic	0.167
Friction angle ϕ	Deterministic	30 degree
Cohesion c	Stochastic	0.577 MPa
Tensile strength T_{f}	Stochastic	0.448 MPa
Hardening parameter α	Deterministic	1.05
Hardening parameter e_{y}	Deterministic	0.0002
Fracture energy G_{f}	Stochastic	10.6 N/m
Softening parameter e_{r}	Deterministic	0.4
Dilatancy coefficient D_{c}	Deterministic	-0.4
Localization size t_{s0}	Deterministic	0.6 mm
Characteristic length l_{c}	Deterministic	100 mm

The loading process consists of the self-weight and active earth pressure loadings. First, the self-weight calculated from the density and the gravitational acceleration was applied in 10 steps. Second, the active earth pressure was applied in 100 steps. The energy norm was used as the convergence criterion in the iteration calculation. The convergence criterion value is

0.0002 and the maximum iteration number is 100. No convergence of the iteration process was judged as the overall failure. 100 realizations were analyzed for θ_{quf} = 0.2 m and 1.0 m.

An example of the q_{uf} distribution for the DCM column model with θ_{quf} = 1.0 m is shown in Figure 3. The histogram of q_{uf} in this model is shown in Figure 4. The mean of q_{uf} is 1.74 MPa and the standard deviation of q_{uf} is 0.485. Since the spatial correlation is considered in the generation of the random field, the statistical parameters of each realization differ from those of the population. The DCM column having a homogeneous strength was also analyzed to determine the equivalent strength for each excavation depth at failure.

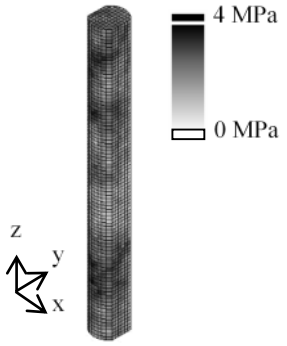

Figure 3. Example of strength distribution for DCM column model with θ_{quf} = 1.0 m.

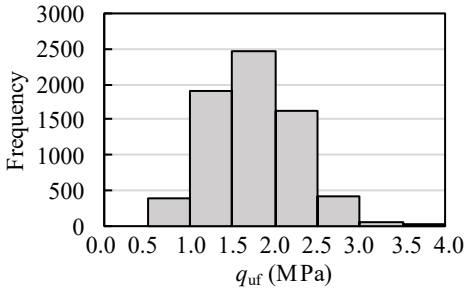

Figure 4. Histogram of q_{uf} for the realization shown in Figure 3

3 NUMERICAL ANALYSIS RESULTS

3.1 *Homogeneous strength column*

The FEM result of the DCM column with the homogeneous strength is shown in Figure 5, 6 and 7. q_{uf} of the DCM column is 1.79 MPa and the excavation depth is 3 m. Figure 5 shows the subgrade reaction of the ground at the excavation side.

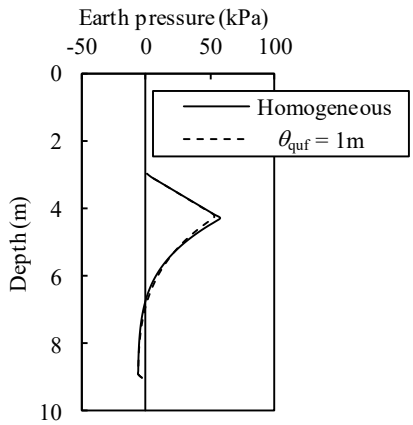

Figure 5. Subgrade reaction of ground at excavation side.

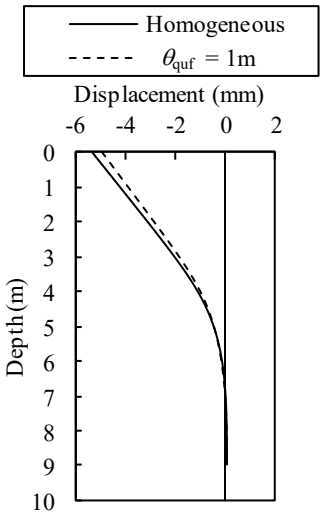

Figure 6. Horizontal displacement of DCM column.

The subgrade reaction reaches the passive earth pressure shallower than 4.3m. Figure 6 shows the horizontal displacement of the DCM column. The horizontal displacement is 0.9 mm at the depth of 4.3m. The horizontal displacement at this depth reasonably agree with that assumed for evaluating the k_h value.

Figure 7 shows the distribution of the normal stress in the z direction just before the failure. The tensile failure occurs at the depth of 4.5 m. That depth corresponds approximately to the lowest depth of the range where the subgrade reaction reaches the passive earth pressure.

Figure 8 shows the unconfined compressive strength of the DCM column which fails at each excavation depth. This relationship indicates the strength required for the homogeneous DCM column at each excavation depth.

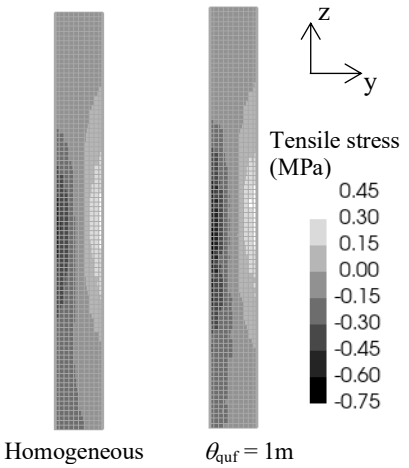

Figure 7. Distribution of normal stress in z direction.

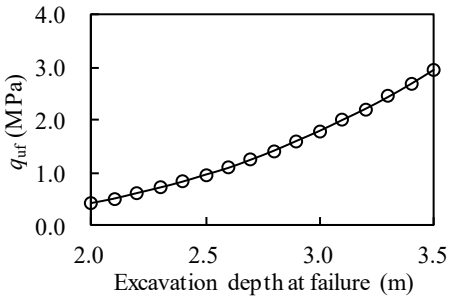

Figure 8. Relationship between unconfined compressive strength q_{uf} and excavation depth at failure of DCM wall.

3.2 *DCM column with spatial variability of strength*

An example of the analysis results for the model with the spatial variability of q_{uf} is shown in Figure 5, 6, and 7. These results show the analysis results for θ_{quf} = 1.0 m. In this example, the DCM column failed at the excavation depth of 3.0 m. Figure 5, and 6 show the earth pressure applied to the DCM column at the excavation side just before the failure and the horizontal displacement of the DCM column. Figure 7 shows the distribution of the normal stress in the z direction just before the failure. The analysis results of the DCM column with the spatial variability of strength do not significantly differ from those of the homogeneous DCM column. This indicates that when V_{quf} = 0.3, the spatial variability of q_{uf} does not significantly affects the distribution of the subgrade reaction at the excavation side and the horizontal displacement of the DCM column.

The DCM columns with the spatial variability of strength failed at the various depth of the excavation. The empirical cumulative distribution function (ECDF) of the excavation depth at which the DCM columns fail is shown in Figure 9. The interval of the excavation depth is 0.1 m. The failure probability calculated by the RFEM analysis can be used in the reliability-based design of the unbraced-unreinforced DCM wall. According to Eurocode 7 (CEN 2004), the characteristic value of the strength is defined as the 5% fractile value of the probability distribution of the overall strength. When the failure probability is set to be 5 %, the excavation depth of 2.6 m is allowable for the DCM column with μ_{quf} = 2.0 MPa, V_{quf} = 0.3 and θ_{quf} = 1 m. Figure 8 shows that the homogeneous DCM column with q_{uf} = 1.08 MPa fails at the excavation depth of 2.6 m. This indicates that the characteristic value of the strength for the DCM column with μ_{quf} = 2.0 MPa, V_{quf} = 0.3 and θ_{quf} = 1 m is 1.08 MPa in the reliability-based design.

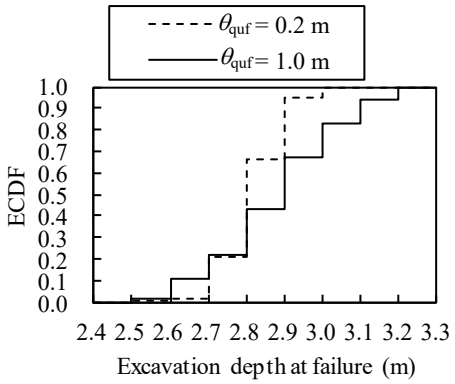

Figure 9. Empirical cumulative distribution function (ECDF) of excavation depth at failure.

3.3 *Current design strength and excavation depth at failure*

The excavation depth at failure for the design strength evaluated in the current design procedure is examined based on the RFEM analysis results. In the current design procedure in Japan (Kitazume and Terashi 2013), the design strength q_{uck} of the cement-treated soil is defined as follow:

$$q_{uck} = \mu_{quf} - K\sigma_{quf} \quad (4)$$

where K is the coefficient derived from the defect rate. In the design procedure in Japan, assuming the normal distribution for q_{uf}, K is normally set to be 1.3 for a 15% - fractile. When μ_{quf} = 2.0 MPa, σ_{quf} = 0.6 MPa and K = 1.3, q_{uck} = 1.22 MPa. The safety factor F_s = 3.0 is normally used for the ordinary condition. Then the allowable compressive strength is 0.407 MPa for the DCM columns with μ_{quf} = 2.0 MPa and σ_{quf} = 0.6 MPa.

Figure 8 shows the relationship between the excavation depth at the failure and the compressive strength of the DCM wall. On the basis of the results shown in Figure 8, the excavation depth at the failure for the allowable strength (0.407 MPa) is about 2.0 m. The RFEM analysis results (Figure 9) shows that the failure probability of the DCM wall with μ_{quf} = 2.0 MPa and σ_{quf} = 0.6 MPa is almost 0 %. This indicates that the allowable strength evaluated by the current design method is too conservative for the design of the unbraced-unreinforced DCM wall. The DCM wall could be design more rationally using the RFEM analysis results.

4 CONCLUSIONS

The RFEM analysis was conducted to investigate the failure behavior of the unbraced-unreinforced DCM wall. The single-row DCM wall with the spatial variability of the strength was analyzed to investigate the effect of the spatial variability on the excavation depth at the failure. The RFEM analysis provides the failure probability of the DCM wall with the spatial variability of the strength at each excavation depth. The spatial correlation affects the empirical cumulative distribution function of the excavation depth of failure. The failure probability calculated by the RFEM analysis can be used in the reliability-based design of the unreinforced DCM wall. The analysis results indicate that the allowable strength calculated with the current design method in Japan is too conservative for the design of the unreinforced DCM wall.

5 REFERENCES

European Committee for Standardization (CEN) 2004. Eurocode 7: Geotechnical Design. Part 1: General Rules, EN 1997-1, Brussels.

Fenton, G.A., and Griffiths, D.V. 2008. Risk Assessment in Geotechnical Engineering. John Wiley & Sons, Inc., New Jersey, USA.

Honjo, Y., Zaika, Y., and Pokharel, G. 2005. Estimation of subgrade reaction coefficient for horizontally loaded piles by statistical analysis. *Soils and Foundations* 45(3), 51-70.

Jamsawang, P., Jamnam, S., Jongpradsit, P., Tanseng, P., and Horpibulsuk, S. 2017. Numerical analysis of lateral movement and strut force in deep cement mixing walls with top-down construction in soft clay. *Computers and Geotechnics* 88, 174-181.

Kitazume, M., and Terashi, M. 2013. The Deep Mixing Method. CRC PressTaylor & Francis Group, London, UK.

Liu, Y., Lee, F.H., Quek, S.T., Chen, E.J., and Yi, J.T. 2015. Effect of spatial variation of strength and modulus on the lateral compression response of cement-admixed clay slab. *Geotechnique* 65(10), 851-865.

Namikawa, T. 2021. Probabilistic analysis of overall strength of a cement-treated soil column considering statistical uncertainty and spatial variability. *International Journal for Numerical and Analytical Methods in Geomechanics* 45, 794-814.

Namikawa, T. 2022. Influence of statistical sample size on evaluation of overall strength of cement-treated soil column. *Canadian Geotechnical Journal* 59, 74-86.

Namikawa, T., and Mihira, S. 2007. Elasto-plastic model for cement-treated sand. *International Journal for Numerical and Analytical Methods in Geomechanics* 31, 71-107.

Pan, Y., Shi, G., Liu, Y., and Lee, F.H. 2018. Effect of spatial variability on performance of cement-treated soil slab during deep excavation. Construction and Building Materials 188, 505-519.

Toraldo, C., Modoni, G., Ochmanski, M., and Croce, P. 2018. The characteristic strength of jet-grouted material. *Geotechnique* 68(3), 262-279.

Waichita, S., Jongpradist, P., and Jamsawang, P. 2019. Characterization of deep cement mixing wall behavior using wall-to-excavation shape factor. *Tunnelling and Underground Space Technology* 83, 243-253.